Water-soluble NHC Pd/Ni bimetallic nanoparticles for H/D exchange in aromatic amino-acids

Oscar Suárez-Riaño, Gabriel Mencia, Simon Tricard, Jerome Esvan, Pier-Francesco Fazzini, Bruno Chaudret, Edwin A Baquero

Water-Soluble NHC-Stabilized Palladium/Nickel Bimetallic Nanoparticles for H/D Exchange Through C–H Bond Activation

Oscar Suárez-Riaño,[a] Gabriel Mencia,*[b] Simon Tricard,[b] Jerome Esvan,[c] Pier-Francesco Fazzini,[b] Bruno Chaudret,[b] and Edwin A. Baquero*[a]

Chem. Commun., 2023, 59, 1062 ; DOI: 10.1039/d2cc06019a

[a] *Estado Sólido y Catálisis Ambiental (ESCA), Departamento de Química, Facultad de Ciencias, Universidad Nacional de Colombia, Carrera 30 No. 45-03, 111321, Bogotá, Colombia. E-mail: eabaquerov@unal.edu.co*
[b] *LPCNO, Laboratoire de Physique et Chimie de Nano-Objets, UMR, 5215 INSA-CNRS-UPS, Institut National des Sciences Appliques 135, Avenue de Rangueil, 31077, Toulouse, France. E-mail: menciabe@insa-toulouse.fr*
[c] *Institut Carnot – Centre Inter-universitaire de Recherche et d'Ingénierie des Matériaux, INP-ENSIACET, CNRS, Université de Toulouse, 118 Route de Narbonne, 31062, Toulouse, France*
Electronic Supplementary Information (ESI) available: Synthetic procedures, characterization data, and NMR spectra of products. See DOI: https://doi.org/10.1039/d2cc06019a

Labelling of amino-acids is important for the production of deuterated proteins. However, aromatic amino-acids reduction is a common undesired process with noble-metal nanocatalysts. In this work, we describe a new NHC-stabilized water-soluble Pd/Ni system able to perform H/D exchange reactions in an enantiospecific fashion without reducing the aromatic ring of phenylalanine and tyrosine thanks to a synergetic Pd-Ni effect.

In recent years, Hydrogen Isotope Exchange (HIE) reactions has gained interest due to the diverse applications of deuterium-labeled compounds in mechanistic studies,[1] alteration of pharmacokinetic profiles of some drugs,[2] as well as internal standards for chromatography.[3] Late stage deuteration proceeds through C–H bond activation, in contrast to other synthetic pathways towards deuterated molecules (deuterated starting materials, building blocks, etc.).[4] In this sense, homogeneous catalysts of noble transition metals (Ir, Ru, Rh, Pd, and Pt)[5] and base metals (Ni, Co, and Fe)[6] together with heterogeneous catalysts of Pd, Pt and Ru,[7] supported on carbon, have been found to be effective in HIE reactions of several substrates through C–H bond activation.[8]

The use of mono- and bi-metallic nanoparticles (NPs) in HIE has been growing due to their high activity and selectivity in the process.[5] This is possible thanks to the presence of adequate ligands on the NP surface which modulate their activity and selectivity. In this sense, *N*-Heterocyclic Carbene (NHC) ligands have been found to be excellent NP stabilizers[9] thanks to their ability to form robust bonds with metals. Thus, we have reported the use of water-soluble Ru@NHC NPs for the selective deuteration of L-lysine at controlled pHs.[10] Further, PdNPs have been employed in HIE using 4-dimethylaminopyridine (DMAP)[11] and polyvinylpyrrolidone (PVP)[12] as stabilizers. However, PdNPs may undergo reduction reactions rather than H/D exchange in aromatic substrates such as *p*-cymene.[13] In contrast, some of us have reported the use of Ni@NHC NPs for the chemoselective H/D exchange in 2-phenylpyridine with full suppression of the reduction side process.[14] Nonetheless, the extension of this protocol to aromatic amino acids (*e.g.* L-phenylalanine) has not been possible so far. It is likely due to the low stability of NiNPs in hydrophilic media. In this sense, synergistic effects may appear in bimetallic systems when two metals combine their beneficial properties in catalytic processes.[15] For example, we have reported recently the use of bimetallic RuPt@NHC[16] and RuIr@NHC NPs[17] for selective H/D exchange in which synergistic effects of both metals have been evidenced. Although bimetallic PdNiNPs have been synthesized[18] and employed as nanocatalysts in methanol and formic acid electro-oxidation,[19] Suzuki-Miyaura,[20] C–O oxidation,[21] and C–C, C–O and C–N coupling reactions,[22] among others, to the best of our knowledge, there are no reports in HIE.

Herein, we report the preparation and characterization by state-of-the-art techniques of new water-soluble PdNiNPs stabilized by NHC ligands (**Pd_xNi_{100-x}@IMesPrSO$_3$**, x = 0, 30, 50, 70, 100) (**Erreur ! Source du renvoi introuvable.**) and their use in the deuteration of L-phenylalanine and L-tyrosine. Remarkably no reduction occurs in this case and the deuteration occurs enantiospecifically at the CH_2-β position with respect to the amino acid group. Monometallic Pd (**Pd)** and Ni (**Ni**) NPs were synthesized by decomposition of $Pd_2(dba)_3$ (dba = dibenzylideneacetone) and $Ni(COD)_2$ (COD = 1,5-cyclooctadiene) adapting procedures previously described for both metals using NHC ligands as stabilizers (see Electronic Supplementary Information for details).[14,23] In order to study the effect of both metals in H/D exchange reactions, bimetallic NPs were prepared by co-decomposition of both precursors, using Pd:Ni molar ratios of 30:70 (**$Pd_{30}Ni_{70}$@IMesPrSO$_3$**), 50:50 (**$Pd_{50}Ni_{50}$@IMesPrSO$_3$**), and 70:30 (**$Pd_{70}Ni_{30}$@IMesPrSO$_3$**), according to their phase diagram.[24] The NPs were stabilized by the addition of a water-soluble NHC ligand namely 1-(2,4,6-trimethylphenyl)-3-(3-potassium sulfonate-propyl)-imidazol-2-ylidene (**IMesPrSO$_3$**) (see Electronic Supplementary Information for details) (Scheme 1).

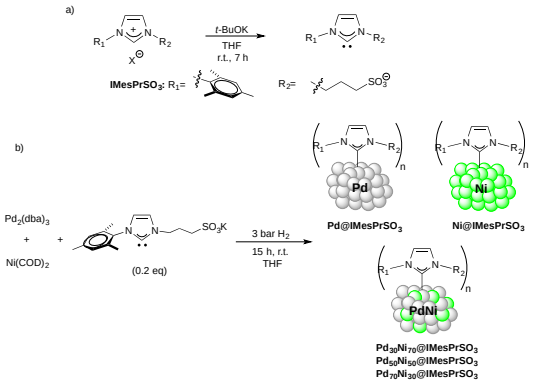

Scheme 1. a) Synthesis of **IMesPrSO$_3$**, and b) Synthesis of Pd, Ni and PdNi NPs stabilized by **IMesPrSO$_3$**.

The resulting NPs were found to disperse and to give rise to colloidal solutions stable for months in water. Transmission Electron Microscopy (TEM) analyses displayed well-dispersed and homogeneous small Pd, Ni and PdNiNPs (1.8–2.9 nm) (Figure 1a, and S4–S7; Table S2). These values are comparable to those previously reported for palladium and nickel NPs functionalized by similar ligands.[14,25,26] Due to their small size,[27] it was not possible to observe clearly the expected face centered cubic (fcc) structure for both Pd and Ni by X-Ray Diffraction (XRD) means (Figures S1–S3). However, further study of the diffraction angle of the 111 lattice shows a quasi-linear relationship between these values and the Pd:Ni ratio (Figure SX). This result is in good agreement with Vegard's law which predicts a linear variation of the diffraction angles from the value of a pure metal to the other in alloys.(ref will be provided) Although we cannot confirm the ordered structure of an alloy, this behavior proves, at least, the bimetallic nature of the NPs. To confirm this, High Resolution (HR)-TEM measurements were carried out for **Pd@IMesPrSO$_3$** (Figure S8), **Pd$_{70}$Ni$_{30}$@IMesPrSO$_3$** (Figure 1b), and **Pd$_{50}$Ni$_{50}$@IMesPrSO$_3$** (Figure S9). Using a Fast Fourier Transformation (FFT) and Energy-Dispersive X-ray spectroscopy (EDX) analysis, monometallic PdNPs with a fcc crystalline structure was confirmed (Figures S8 and S10, respectively). Regarding bimetallic PdNiNPs, the analysis showed that the crystalline structure for **Pd$_{70}$Ni$_{30}$@IMesPrSO$_3$** NPs was compatible with the cubic Pd structure (Figure 1b). In contrast, the crystalline structure of **Pd$_{50}$Ni$_{50}$@IMesPrSO$_3$** NPs was not possible to be determined by FFT analysis, due to their irregular shape (Figure S9). In order to confirm the bimetallic nature of the NPs observed by XRD, High-Resolution Scanning Transmission Electron Microscopy (STEM) coupled to EDX technique was performed on the **Pd$_{70}$Ni$_{30}$@IMesPrSO$_3$** and **Pd$_{50}$Ni$_{50}$@IMesPrSO$_3$** samples. STEM in high-angle annular dark field (HAADF), obtained with an atomic resolution microscope (ARM), showed that these samples are indeed PdNi bimetallic systems (Figure 1 and S13 change figures (An overlap of the elemental mapping with the HAADF could help the referees)). It was confirmed by EDX where Pd:Ni molar ratios of 72:28 and 58:42 was observed for **Pd$_{70}$Ni$_{30}$@IMesPrSO$_3$**, and **Pd$_{50}$Ni$_{50}$@IMesPrSO$_3$**, respectively (Figures S11–S12). Further, Inductively Coupled Plasma Atomic Emission Spectroscopy (ICP-AES) confirmed the expected values for all bimetallic systems (Table S1). These results are in agreement with the formation of bimetallic PdNiNPs.

Surface state studies of MNPs using CO adsorption experiments were carried out to evaluate the availability and accessibility of the metal atoms on the surface. The straightforward coordination of carbon monoxide to the Pd and Ni surface allows the determination of the open sites. It may coordinate in a bridging (CO_b, on the faces of the NP) or in a terminal mode (CO_t, on the apexes and edges of the NP). Thus, Pd, Ni and PdNiNPs were exposed to 1 bar of CO overnight and their Attenuated Total Reflectance Fourier Transform Infrared (ATR FT-IR) spectra were recorded (Figure S14). We observe that both **Pd@IMesPrSO$_3$** and **Ni@IMesPrSO$_3$** NPs have both CO_b and CO_t modes at ~ 1900 cm^{-1} and ~ 2020 cm^{-1} for Pd, and ~ 1950-1970 cm^{-1} and ~ 2050 cm^{-1} for Ni, respectively. Concerning bimetallic systems, both CO_b signals from Pd and Ni appear, as well as the CO_t vibration as broad peaks due to the proximity of the signals from the Pd-based and Ni-based systems. In addition, when increasing the palladium content in the bimetallic systems, we observe that the CO_b frequency shifts gradually to lower wavenumbers, close to the one of the monometallic Pd NPs (1914, 1907, and 1899 cm^{-1} for **Pd$_{30}$Ni$_{70}$@IMesPrSO$_3$**, **Pd$_{50}$Ni$_{50}$@IMesPrSO$_3$**, and **Pd$_{70}$Ni$_{30}$@IMesPrSO$_3$**, respectively). Since CO IR bands are sensitive to the environment and the metals present (ref) in the surface, this shift must be related to a change in the electronic properties of Pd due to the presence of Ni. This same effect can be observed in the Pd CO_t band which is shifted from 2020 cm^{-1} to 2032 cm^{-1}, 2035 cm^{-1} and 2039 cm^{-1} when the Ni content is increased. These results demonstrate that the surface of the NPs is available for coordination and suggest the presence of both metals at the surface of a same nanoparticle confirming their bimetallic nature.

Moreover, Solid-State NMR (SS-NMR) measurements were carried out to verify the NHC coordination over the NP surface. We recorded the $^{1}H–^{13}C$ Cross Polarization Magic Angle Spinning (CP-MAS) SS-NMR spectrum for the different MNPs. For **Pd@IMesPrSO$_3$** NPs (Figure S16, black), a resonance signal at 164 ppm might be attributed to a non-Knight-shift carbenic carbon of the NHC ligand linked to Pd.[25] In addition, signals from the aromatic ring, the imidazole moiety, the alkyl sulfonate chain, and the methyl substituents were observed at 134, 128, 40–30, and 20 ppm, respectively. Regarding bimetallic PdNiNPs, we were able to record the ^{13}C MAS SS-NMR spectrum only with **Pd$_{70}$Ni$_{30}$@IMesPrSO$_3$** NPs. However, no signal corresponding to Pd-C_{NHC} or Ni-C_{NHC} carbenic carbons was detected (Figure S15). It can be due to the presence of Knight shift given the size of the NPs (2.6 nm, see Table S2) and/or to the magnetic nature of Ni.

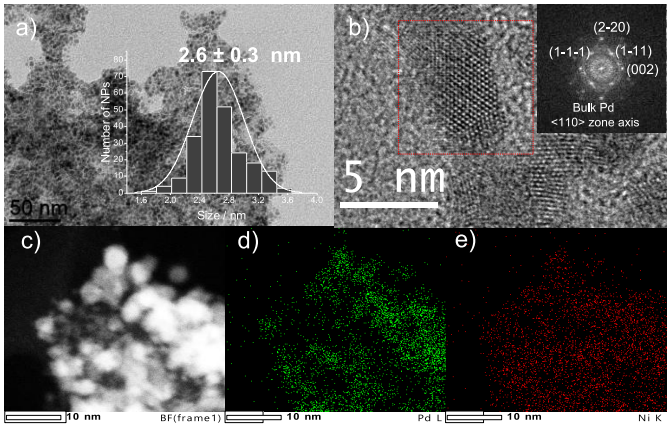

Figure 1. a) TEM (inset: size distribution), b) HR-TEM and FFT analysis (inset), c) HR-STEM-HAADF image of **Pd$_{70}$Ni$_{30}$@IMesPrSO$_3$**, and (d-e) Elemental mapping.

Additionally, we exposed the **Pd@IMesPrSO$_3$** NPs to 1 bar of ^{13}CO overnight and recorded the ^{13}C MAS and $^{1}H–^{13}C$ CP-MAS SS-NMR spectra (Figure S16, blue and red). As it can be observed, two new resonance signals appeared at 160 and 210 ppm corresponding to $^{13}CO_t$ and $^{13}CO_b$, respectively.[28] It should be noted that the $^{13}CO_b$ signal has higher intensity in the ^{13}C MAS compared to the $^{1}H–^{13}C$ CP-MAS spectrum. In the latter experiment, protons can transfer polarization to near ^{13}C nuclei. Consequently, these ^{13}C will enhance their intensity if the heteronuclear coupling contact time is longer than the NMR time scale. Thus, a loss of the signal intensity of $^{13}CO_b$ suggests that they are highly mobile. On the contrary, the $^{13}CO_t$ resonance signal is enhanced in the CP-MAS experiment. These results point out two important features: i) the faces of the NPs are totally available for coordination of, for example, substrates which is crucial for catalysis, and ii) the NHC ligands are coordinated at the edges of the NPs avoiding the mobility of the $^{13}CO_t$ coordinated preferentially at the corners of the NP.[29] Unfortunately, our efforts to perform this experiment on PdNiNPs were not successful likely because of magnetism of Ni.

In addition, X-ray Photoelectron Spectroscopy (XPS) has been presented as an alternative to observe the coordination mode of the stabilizing ligands on the metal surface.[10,30] Thus, XPS was performed on the samples **Pd@IMesPrSO$_3$**, **Pd$_{50}$Ni$_{50}$@IMesPrSO$_3$**, and **Ni@IMesPrSO$_3$**. By observing the change in the binding energy of the N1s signals from imidazolium salt **IMesPrSO$_3$H** (~ 401 eV), compared to **Pd@IMesPrSO$_3$**, **Pd$_{50}$Ni$_{50}$@IMesPrSO$_3$**, and **Ni@IMesPrSO$_3$** (~ 399 eV) (Figure S17), we can conclude that NPs are stabilized by NHC coordination and not by electrostatic interactions with the imidazolium salt.[10] This coordination, usually strong, explains the high colloidal stability in water observed for these NPs.[31]

Taking into account the importance of deuterated biomolecules, the water-soluble mono- and bi-metallic NPs were used as nanocatalysts in HIE reactions using three different amino acids (L-phenylalanine, L-tyrosine, and L-histidine) as substrates.[32] Additionally, these amino acids were chosen to study the selectivity in H/D exchange *vs.* the aromatic ring reduction. In Table 1 we summarize the results obtained with L-phenylalanine as a substrate. H/D exchange was observed only in the CH_2-β position with respect to the amino acid group of the substrate. Such a selectivity contrasts with the previously reported selectivity with amino acids using Ru-based NPs, where the CH-α position is usually deuterated.[10,16,33] This effect is caused by Pd, as it has been observed previously in phenylalanine derivatives using Pd/C.[34] Low deuterium incorporation was obtained when monometallic **Pd@IMesPrSO$_3$** and **Ni@IMesPrSO$_3$** NPs were used as nanocatalysts (Table 1, Entries 1 and 5, respectively). It should be noted that no reduction of the aromatic ring was observed using **Pd@IMesPrSO$_3$**. Surprisingly, although Pd NPs showed a very low activity, Pd-enriched bimetallic **PdNi@IMesPrSO$_3$** NPs displayed better activities (Table 1, Entries 2 and 3), with better activities when Pd content is increased, **Pd$_{70}$Ni$_{30}$@IMesPrSO$_3$** being the best catalyst of the series with 98.5 % of deuterium incorporation on CH_2-β in our standard conditions (Table 1, Entry

2). This result can be due to changes in the polarization of the surface as observed by the changes in the CO band with Pd:Ni ratio. It is also worth to mention that in general similar proportions of the different diastereoisomers is observed. This fact suggests that the conversion rates from one specie to the other must be similar and low. In the case of **$Pd_{70}Ni_{30}$@IMesPrSO$_3$**, the activity is high enough to convert almost all the substrate into its CD_2-β version in the reaction time. These results clearly show a beneficial synergetic effect, in which an enhanced activity is observed when bimetallic PdNiNPs were used compared to the monometallic versions.[15] Remarkably, based on NMR studies (see Electronic Supplementary Information for details, Figures S27–S29), we found that the first deuteration of the CH_2-β position took place in an enantiospecific fashion in all experiments. Thus, the first step of the H/D exchange afforded exclusively (*2S, 3R*)-3-(^{2}H)-phenylalanine (Scheme S6),[35] even when we performed the experiment using **$Pd_{50}Ni_{50}$@IMesPrSO$_3$** as a nanocatalyst during 16 h of reaction with low deuterium incorporation (Table 1, Entry 6).

).

Table 1. H/D exchange in L-phenylalanine using MNPs as nanocatalysts.[a]

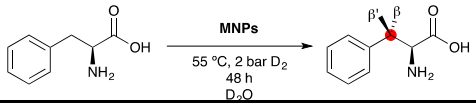

Entry	MNPs	Deuterium incorporation (%)[b]		
		CHD (β')	CD_2 (β'+β)	Total
1	**Pd@IMesPrSO$_3$**	2.5	3.0	5.5
2	**$Pd_{70}Ni_{30}$@IMesPrSO$_3$**	1.5	97.0	98.5
3	**$Pd_{50}Ni_{50}$@IMesPrSO$_3$**	24.5	34.0	58.5
4	**$Pd_{30}Ni_{70}$@IMesPrSO$_3$**	6.5	8.0	14.5
5	**Ni@IMesPrSO$_3$**	7.0	12.0	19.0
6[c]	**$Pd_{50}Ni_{50}$@IMesPrSO$_3$**	10.5	10.0	20.5

[a] Reaction conditions: 2 bar D_2 (8.1 mmol, 58 eq.), 55 °C, 48h, 4 mol% catalyst (**PdNi@IMesPrSO$_3$**) or 5 mol% (**Pd@IMesPrSO$_3$**, **Ni@IMesPrSO$_3$**), 0.1399 mmol of substrate, 2 mL of D_2O and pH=8-9. [b] Determined by ^{1}H NMR. [c] Reaction carried out during 16 h.

Table 2. HIE reaction with L-tyrosine using MNPs as nanocatalysts.[a]

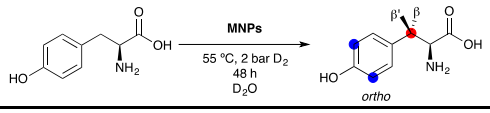

Entry	MNPs	Deuterium incorporation (%)[b]			
		CHD (β')	CD_2 (β'+β)	Total	*ortho*
1	**$Pd_{30}Ni_{70}$@IMesPrSO$_3$**	10.0	14.0	24.0	-
2	**$Pd_{50}Ni_{50}$@IMesPrSO$_3$**	9.0	11.0	20.0	-
3	**$Pd_{70}Ni_{30}$@IMesPrSO$_3$**	8.5	21.0	29.5	-
4[c]	**$Pd_{70}Ni_{30}$@IMesPrSO$_3$**	5.0	4.0	9.0	70.0

[a] Reaction conditions: 2 bar D_2 (8.1 mmol, 58 eq.), 55 °C, 48h, 4 mol% catalyst (**PdNi@IMesPrSO$_3$**), 0.1399 mmol of substrate, 2 mL of D_2O and pH=11-12. [b] Determined by ^{1}H NMR. [c] Reaction carried out at 120 °C.

Results using L-tyrosine as a substrate are summarized in Table 2. Only bimetallic systems were evaluated with this substrate. Similarly to phenylalanine, the first deuteration was found to be enantiospecific. Additionally, lower deuterations were observed using this substrate compared to L-phenylalanine (Table 2, Entries 1–3). Moreover, no significant trend was found related to Pd:Ni composition. This may be related to the hydroxyl group which can change the coordination mode of tyrosine on the NP surface. In order to obtain better results, an experiment at 120 °C was performed using **$Pd_{70}Ni_{30}$@IMesPrSO$_3$** as a nanocatalyst. Remarkably, the deuterium labelling site changed to the *ortho* position to the hydroxyl group, with moderate activity under the catalytic conditions (Table 2, Entry 4). Similar results were obtained using Pd/C catalyst[34] but with a lower activity. This result suggests likely a different coordination mode of this substrate to the NP surface. At lower temperature, the amino acid moiety is coordinated to the surface. Thus, the CH_2-β position points towards the nanoparticle's surface facilitating its H/D exchange. In contrast, at higher temperature the phenol group is likely coordinated to the surface assisting the H/D exchange of the close *ortho* C–H bonds. Therefore, this selectivity can be tuned by changing the temperature of the reaction using L-tyrosine as a substrate.

Finally, the last amino acid studied was L-histidine. It is important to notice that the B position of the L-histidine (Table S3) was easily fully deuterated in all the experiments performed, even in the absence of any nanocatalyst (Table S3, Entry 1). Transition metal free H/D exchange of L-histidine using deuterated hydrochloric,[36] and trifluoromethanesulfonic acids[37] as deuterium sources has previously been reported. Nevertheless, when using **Pd@IMesPrSO$_3$**, **Ni@IMesPrSO$_3$** and, **Pd$_{70}$Ni$_{30}$@IMesPrSO$_3$**, differences in deuteration at the A position were found, with better results obtained when Pd-based systems were used as nanocatalysts (Table S3, Entries 3 and 4). It is worth mentioning that the better result was obtained with **Pd$_{70}$Ni$_{30}$@IMesPrSO$_3$**, showing again a beneficial synergetic effect.

Conclusions

Different new water-soluble NHC-stabilized mono- and bi-metallic PdNiNPs were synthesized and characterized. Their high colloidal stability is explained by the coordination of the NHC ligand to their surface, confirmed by means of XPS and solid-state NMR. The bimetallic nature of the PdNiNPs was confirmed by XRD, STEM-EDX and ATR-FTIR studies. The bimetallic PdNiNPs were studied in H/D exchange reactions leading to five important observations: i) the bimetallic nature of the NPs leads to an important increase in L-phenylalanine deuteration evidencing the presence of a beneficial synergistic effect, especially for the composition **Pd$_{70}$Ni$_{30}$@IMesPrSO$_3$**; ii) no reduction of the phenyl rings of the amino acids was observed; iii) H/D exchange occurs exclusively on the CH_2-β position, evidencing a different mechanism than that observed with the other amino-acids where the CH-α position is deuterated; iv) the first H/D exchange step was found to be enantiospecific based on NMR studies, and v) the same nanocatalyst allowed us to control the selectivity in the deuterium labelling position in L-tyrosine just by adjusting the temperature of the reaction. These results illustrate the importance of the structure of nanocatalysts, here bimetallic PdNi NPs for the selectivity of H/D exchange in biologically relevant molecules.

Acknowledgements

This work was supported by the Universidad Nacional de Colombia and DIEB (Project with HERMES code 56495), H2020/FET- Open FLIX-862179, and ERC-AdG MONACAT 694159. O.S.-R. is grateful to the NanoX Graduate School of Research program for his internship at LPCNO in Toulouse. The authors thank Y. Coppel for solid-state NMR measurements.

Notes and references

1 J. Atzrodt, V. Derdau, W. J. Kerr and M. Reid, *Angew. Chem. Int. Ed.*, 2018, **57**, 1758–1784.
2 A. Katsnelson, *Nat. Med.*, 2013, **19**, 656–656.
3 J. Atzrodt and V. Derdau, *J. Label. Compd. Radiopharm.*, 2010, **53**, 674–685.
4 A. Palazzolo, J. M. Asensio, D. Bouzouita, G. Pieters, S. Tricard and B. Chaudret, in *Recent Advances in Nanoparticle Catalysis*, 2020, pp. 281–302.
5 M. Lepron, M. Daniel-Bertrand, G. Mencia, B. Chaudret, S. Feuillastre and G. Pieters, *Acc. Chem. Res.*, 2021, **54**, 1465–1480.
6 H. Yang and D. Hesk, *J. Label. Compd. Radiopharm.*, 2020, **63**, 296–307.
7 M. Valero and V. Derdau, *J. Label. Compd. Radiopharm.*, 2020, **63**, 266–280.
8 T. Pirali, M. Serafini, S. Cargnin and A. A. Genazzani, *J. Med. Chem.*, 2019, **62**, 5276–5297.
9 H. Shen, G. Tian, Z. Xu, L. Wang, Q. Wu, Y. Zhang, B. K. Teo and N. Zheng, *Coord. Chem. Rev.*, 2022, **458**, 214425.
10 L. M. Martínez-Prieto, E. A. Baquero, G. Pieters, J. C. Flores, E. De Jesús, C. Nayral, F. Delpech, P. W. N. M. Van Leeuwen, G. Lippens and B. Chaudret, *Chem. Commun.*, 2017, **53**, 5850–5853.
11 J. A. Sullivan, K. A. Flanagan and H. Hain, *Catal. Today*, 2008, **139**, 154–160.
12 V. Pfeifer, T. Zeltner, C. Fackler, A. Kraemer, J. Thoma, A. Zeller and R. Kiesling, *Angew. Chem. Int. Ed.*, 2021, **60**, 26671–26676.
13 C. Zhao, W. Gan, X. Fan, Z. Cai, P. Dyson and Y. Kou, *J. Catal.*, 2008, **254**, 244–250.
14 D. Bouzouita, J. M. Asensio, V. Pfeifer, A. Palazzolo, P. Lecante, G. Pieters, S. Feuillastre, S. Tricard and B. Chaudret, *Nanoscale*, 2020, **12**, 15736–15742.
15 A. K. Singh and Q. Xu, *ChemCatChem*, 2013, **5**, 652–676.
16 D. Bouzouita, G. Lippens, E. A. Baquero, P. F. Fazzini, G. Pieters, Y. Coppel, P. Lecante, S. Tricard, L. M. Martínez-Prieto and B. Chaudret, *Nanoscale*, 2019, **11**, 16544–16552.
17 A. Zuluaga-Villamil, G. Mencia, J. M. Asensio, P.-F. Fazzini, E. A. Baquero and B. Chaudret, *Organometallics*, 2022, DOI:10.1021/acs.organomet.2c00288.
18 N. J. S. Costa, M. Guerrero, V. Collière, É. Teixeira-Neto, R. Landers, K. Philippot and L. M. Rossi, *ACS Catal.*, 2014, **4**, 1735–1742.
19 a) L. Chen, H. Guo, T. Fujita, A. Hirata, W. Zhang, A. Inoue and M. Chen, *Adv. Funct. Mater.*, 2011, **21**, 4364–4370. b) Z. Qi, H. Geng, X. Wang, C. Zhao, H. Ji, C. Zhang, J. Xu and Z. Zhang, J. *Power Sources*, 2011, **196**, 5823–5828.
20 Y. Wu, D. Wang, P. Zhao, Z. Niu, Q. Peng and Y. Li, *Inorg. Chem.*, 2011, **50**, 2046–2048.
21 S. Shan, V. Petkov, L. Yang, J. Luo, P. Joseph, D. Mayzel, B. Prasai, L. Wang, M. Engelhard and C.-J. Zhong, *J. Am. Chem. Soc.*, 2014, **136**, 7140–7151.
22 M. Aalinejad, N. Pesyan Noroozi and H. Alamgholiloo, *Colloids Surfaces A Physicochem. Eng. Asp.*, 2022, **634**,

127956.
23 S. Jansat, J. Durand, I. Favier, F. Malbosc, C. Pradel, E. Teuma and M. Gómez, *ChemCatChem*, 2009, **1**, 244–246.
24 ASM International, *ASM handbook volume 3: Alloy phase diagrams*, 1998.
25 J. M. Asensio, S. Tricard, Y. Coppel, R. Andrés, B. Chaudret and E. de Jesús, *Chem. Eur. J.*, 2017, **23**, 13435–13444.
26 J. M. Asensio, S. Tricard, Y. Coppel, R. Andrés, B. Chaudret and E. de Jesús, *Angew. Chem. Int. Ed.*, 2017, **56**, 865–869.
27 S. Mourdikoudis, R. M. Pallares and N. T. K. Thanh, *Nanoscale*, 2018, **10**, 12871–12934.
28 P. Lara, O. Rivada-Wheelaghan, S. Conejero, R. Poteau, K. Philippot and B. Chaudret, *Angew. Chem. Int. Ed.*, 2011, **50**, 12080–12084.
29 I. Cano, L. M. Martínez-Prieto, P. F. Fazzini, Y. Coppel, B. Chaudret and P. W. N. M. Van Leeuwen, *Phys. Chem. Chem. Phys.*, 2017, **19**, 21655–21662.
30 L. M. Martínez-Prieto, I. Cano, A. Márquez, E. A. Baquero, S. Tricard, L. Cusinato, I. del Rosal, R. Poteau, Y. Coppel, K. Philippot, B. Chaudret, J. Cámpora and P. W. N. M. van Leeuwen, *Chem. Sci.*, 2017, **8**, 2931–2941.
31 a) E. A. Baquero, S. Tricard, J. C. Flores, E. de Jesús and B. Chaudret, *Angew. Chem. Int. Ed.*, 2014, **53**, 13220–13224. b) E. A. Baquero, S. Tricard, Y. Coppel, J. C. Flores, B. Chaudret and E. de Jesús, *Dalton Trans.*, 2018, **47**, 4093–4104.
32 A. Palazzolo, S. Feuillastre, V. Pfeifer, S. Garcia-Argote, D. Bouzouita, S. Tricard, C. Chollet, E. Marcon, D. Buisson, S. Cholet, F. Fenaille, G. Lippens, B. Chaudret and G. Pieters, *Angew. Chem. Int. Ed.*, 2019, **58**, 4891–4895.
33 C. Taglang, L. M. Martínez-Prieto, I. del Rosal, L. Maron, R. Poteau, K. Philippot, B. Chaudret, S. Perato, A. Sam Lone, C. Puente, C. Dugave, B. Rousseau and G. Pieters, *Angew. Chem. Int. Ed.*, 2015, **54**, 10474–10477.
34 T. Maegawa, A. Akashi, H. Esaki, F. Aoki, H. Sajiki and K. Hirota, *Synlett*, 2005, 0845–0847.
35 D. W. Barnett, M. J. Panigot and R. W. Curley, *Tetrahedron: Asymmetry*, 2002, **13**, 1893–1900.
36 J. Šamonina-Kosicka and M. Kańska, *J. Label. Compd. Radiopharm.*, 2013, **56**, 317–320.
37 M. Hashimoto, Z. Puteri Tachrim, N. Kurokawa and Y. Tokoro, *Heterocycles*, 2020, **101**, 357.

TOC Content

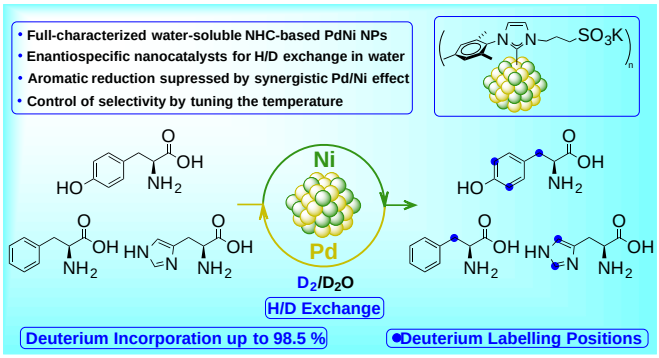

We demonstrate selective and enantiospecific isotopic H/D exchange in aromatic amino acids without ring reduction catalyzed by well-defined water-soluble NHC-stabilized bimetallic PdNi nanoparticles.